Electronic Supplementary Information

Spatial Disposition of Square-Planar Mononuclear Nodes in Metal-Organic Frameworks for C_2H_2/CO_2 Separation

Heng Zeng,‡[a] Xiao-Jing Xie,‡[a] Ying Wang,[a] Dong Luo,[a] Rong-Jia Wei,[a] Weigang Lu,[a,*] and Dan Li[a,*]

[a]College of Chemistry and Materials Science, and Guangdong Provincial Key Laboratory of Functional Supramolecular Coordination Materials and Applications, Jinan University, Guangzhou 510632, P. R. China

Correspondence and requests for materials should be addressed to W.L. (email: weiganglu@jnu.edu.cn) or to D.L. (email: danli@jnu.edu.cn)

Methods

All reagents and solvents were obtained commercially and used as received without further purification. The ligand 5-(3-methyl-5-(pyridin-4-yl)-4H-1,2,4-triazol-4-yl)-1,3-benzenedicarboxylic acid (H_2MPTBDC) was purchased from Shanghai Tensus Bio-tech Co., Ltd. Ultrahigh-purity-grade N_2 (> 99.999%), C_2H_2 (> 99.9%), and CO_2 (> 99.99%) were purchased from Dalian Special Gases.

Preparation of JNU-4: A mixture of $Cu(NO_3)_2 \cdot 3H_2O$ (2.27 mmol, 468 mg), H_2MPTBDC (0.94 mmol, 306 mg), acetonitrile (CH_3CN, 60 mL), deionized water (H_2O, 30 mL), and 0.1 M nitric acid was placed in a sealed glass vial (350 mL) and heated at 120 °C for 12 h. After cooling to room temperature, the dark blue crystals (as-synthesized JNU-4) were collected and washed with methanol 10 times, then filtered and activated under high vacuum at room temperature for 24 hours to afford the activated JNU-4 (JNU-4a, 0.210 g, 67.7 % yield based on H_2MPTBDC). Analytically calculated (found) for $(C_{16}H_{10}Cu_2N_4O_4) \cdot H_2O$: C, 41.12 % (41.08 %); H, 2.59 % (4.49 %); N, 11.99 % (11.78 %).

Gas adsorption measurements

At least 120 mg of sample was used for each measurement. JNU-4a was activated at room temperature under a dynamic vacuum (below 5 μm Hg) for 24 h. Further degassing and single-component adsorption/desorption at different temperatures were conducted on a Micromeritics ASAP 2020 PLUS Analyzer.

Single-crystal X-ray diffraction analysis

Single-crystal diffraction data of JNU-4 was collected at 100 K *via* an Oxford Cryo stream system on a XtaLAB PRO MM007-DW diffractometer system equipped with a RA-Micro7HF-MR-DW (Cu/Mo) X-ray generator and HyPix-6000HE hybrid photon counting X-ray detector (Rigaku, Japan, Cu Kα, λ = 1.5418 Å). The structures were solved and refined using Olex 2 with the 'XS' and 'XL' plugins.

PXRD analysis

PXRD data were collected by using microcrystalline samples on a Rigaku Ultima IV diffractometer (40 kV, 40 mA, Cu Kα, λ = 1.5418 Å). The measurement parameters include a scan speed of 10° min^{-1}, a step size of 0.02°, and a scan range of 2θ from 5° to 30°.

The isosteric heat of adsorption (Q_{st})

The isosteric heat of adsorption for C_2H_2 and CO_2 were calculated by using the gas adsorption data collected at three different temperatures. The adsorption isotherms were first fitted with the viral equation[1]:

$$\ln P = \ln N + \frac{1}{T}\sum_{i=0}^{m} a_i N^i + \sum_{i=0}^{n} b_i N^i$$

Where N is gas uptake (in mg g^{-1}), P is pressure (in mmHg), a and b are virial coefficients, m and n are the numbers of coefficients required to adequately describe

the isotherm. The parameters that were obtained from the fitting of the C_2H_2 and CO_2 adsorption isotherms can be found in Figures S9 and S10. All isotherms were fitted with $R^2 > 0.99$.

The obtained parameters were used to calculate Q_{st} in the range of adsorption capacity through the virial equation, which is as follows:

$$Q_{st} = -\mathrm{R}\sum_{i=0}^{m} a_i N^i$$

IAST calculations of adsorption selectivity

The fitting of C_2H_2 and CO_2 adsorption isotherms were carried out by using the dual-site Langmuir-Freundlich (DSLF) model. Their corresponding fitting parameters are displayed in Table S1. The Ideal Adsorbed Solution Theory (IAST) of Myers and Prausnitz[2] was applied to quantitatively estimate the adsorption selectivity for C_2H_2/CO_2 (50/50) mixture, respectively.

Dual-site Langmuir-Freundlich (DSLF) model is listed as below:

$$\mathrm{q} = q_{A,sat}\frac{b_A P^{1/nA}}{1 + b_A P^{1/nA}} + q_{B,sat}\frac{b_B P^{1/nB}}{1 + b_B P^{1/nB}}$$

Where q is gas uptake (in mmol g^{-1}), P is pressure (in kPa), $q_{A,sat}$ and $q_{B,sat}$ are saturation uptakes (in mmol g^{-1}) for sites A and B, b_A and b_B are affinity coefficients (in kPa^{-1}) for sites A and B, and nA and nB represent the deviations from the ideal homogeneous surface for sites A and B. All isotherms were fitted with $R^2 > 0.999$.

Adsorption selectivity, S_{ads}, is defined for the separation of a binary mixture of component i and j as follows:

$$\mathrm{S}_{ads} = \frac{q_i/q_j}{p_i/p_j}$$

where q_i and q_j represent the molar loadings of component i and j that is in equilibrium; p_i and p_j represent the partial pressures of component i and j in the bulk gas phase.

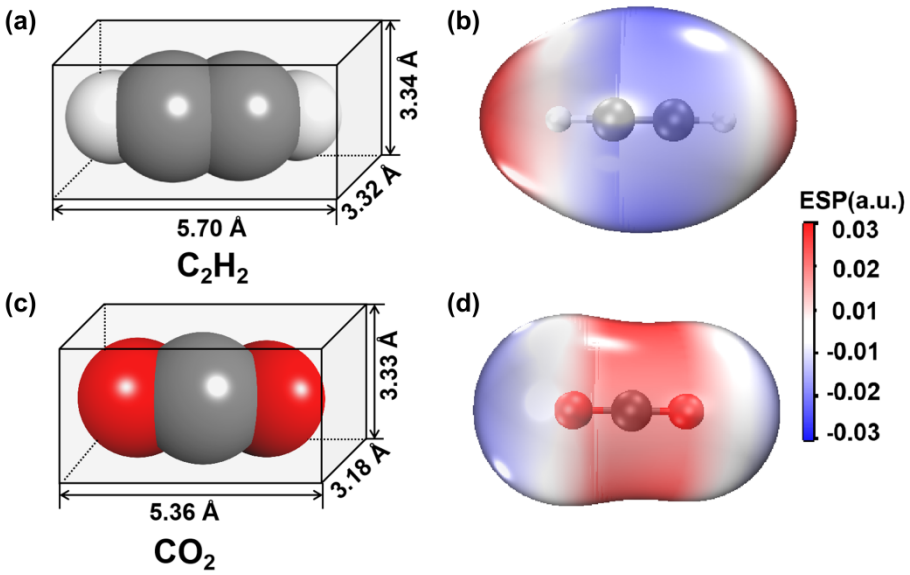

Figure S1. (a) Molecular size and (b) electrostatic potential of C_2H_2. (c) Molecular size and (d) electrostatic potential of CO_2. Electrostatic potential (ESP) analysis was performed by the Multiwfn software package.[3-5]

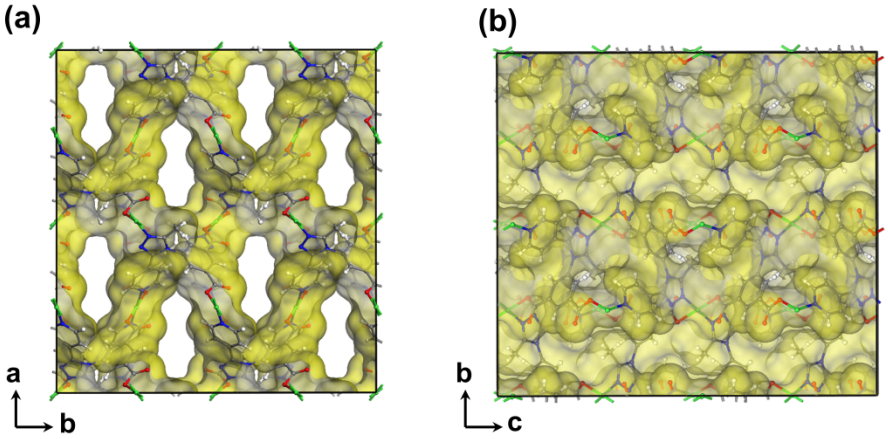

Figure S2. (**a**) Connolly surface representation of JNU-4 viewed along the *c*-axis (yellow/gray curved surface). (**b**) Cross-sectional view of the connolly surface of the pore in **c**, revealing that the densely open Cu sites within the pore surfaces. Color code: Green, Cu; red, O; blue, N; gray, C; white, H.

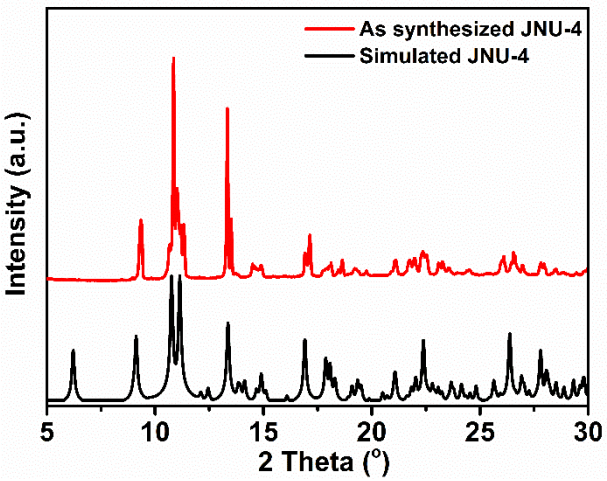

Figure S3. PXRD patterns of the simulated (black) and as-synthesized (red) JNU-4.

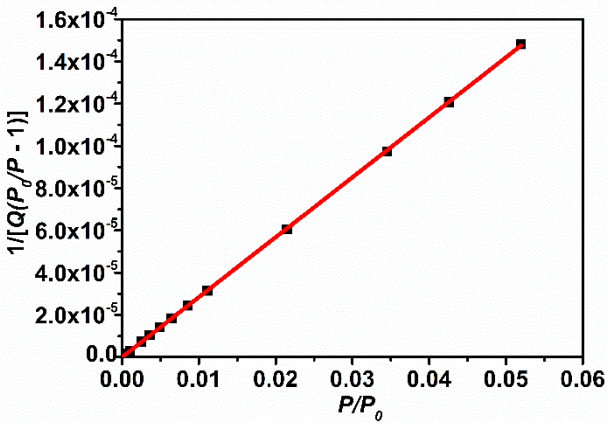

Figure S4. BET plot for surface area calculation.

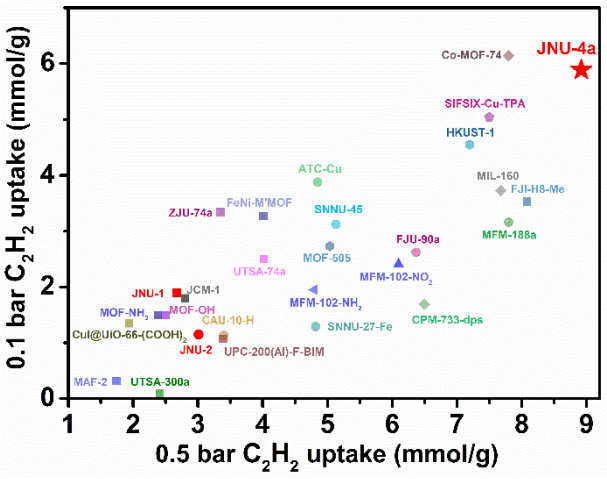

Figure S5. Comparison of C_2H_2 gravimetric capacity at 0.5 and 0.1 bar in JNU-4a and other porous materials at room temperature.

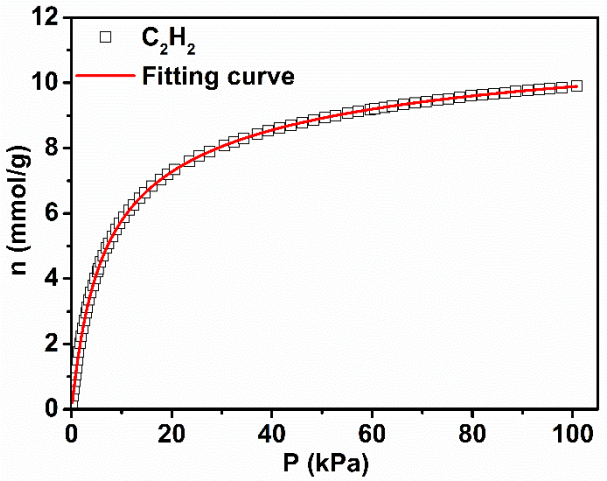

Figure S6. Dual-site Langmuir-Freundlich fitting of the C_2H_2 adsorption isotherm of JNU-4a at 298 K.

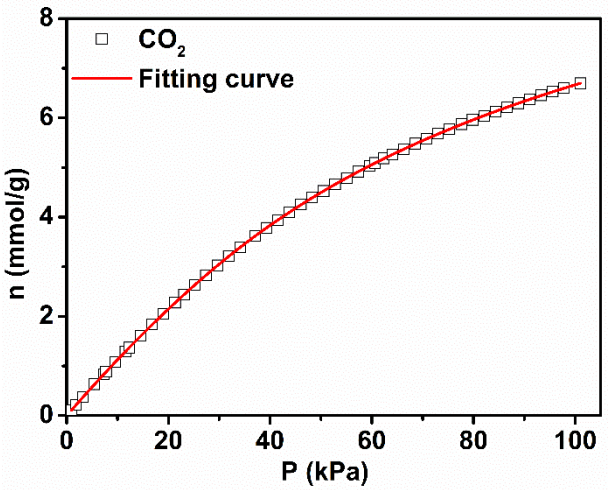

Figure S7. Dual-site Langmuir-Freundlich fitting of the CO_2 adsorption isotherm of JNU-4a at 298 K.

Table S1. Dual-site Langmuir-Freundlich parameters from the fitting of C_2H_2 and CO_2 adsorption isotherms of JNU-4a at 298 K. The R^2 values are also provided.

Parameter	C_2H_2	CO_2
$q_{A,sat}$	4.649	11.92
b_A	0.03131	0.00978
$1/n_A$	0.8948	1.018
$q_{B,sat}$	7.086	0.5649
b_B	0.1862	1.388E-4
$1/n_B$	1.068	2.476
R^2	0.9999	1

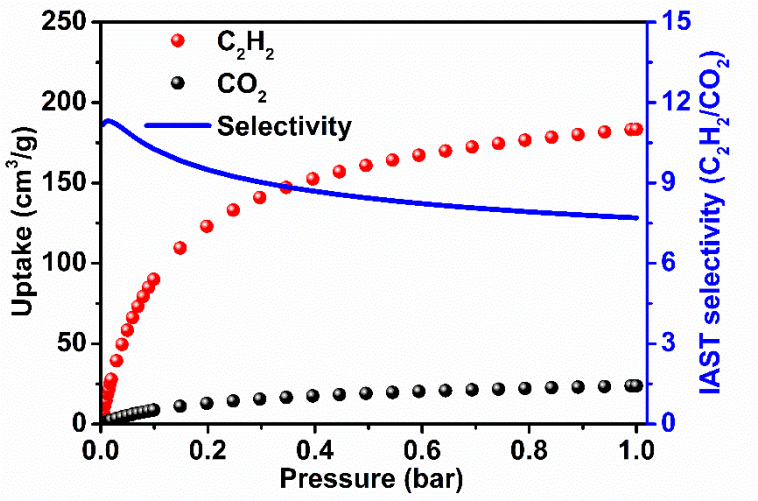

Figure S8. Predicted mixture adsorption isotherms and selectivity of JNU-4a predicted by the IAST method for a 50/50 C_2H_2/CO_2 mixture at 298 K.

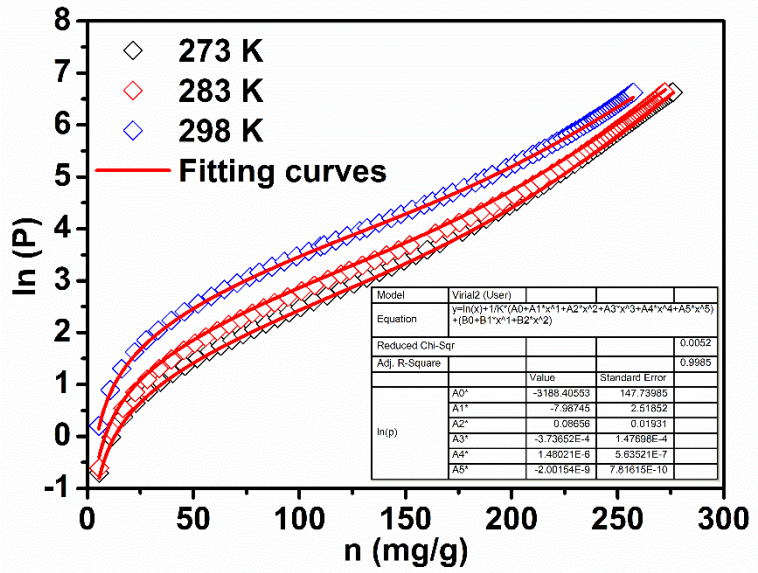

Figure S9. Virial equation fitting of the C_2H_2 adsorption isotherms of JNU-4a at 273, 283, and 298 K.

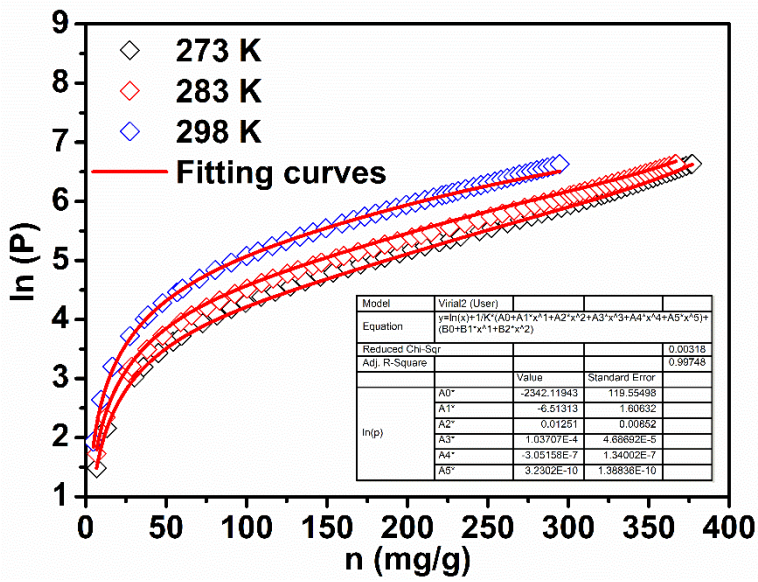

Figure S10. Virial equation fitting of the CO_2 adsorption isotherms of JNU-4a at 273, 283, and 298 K.

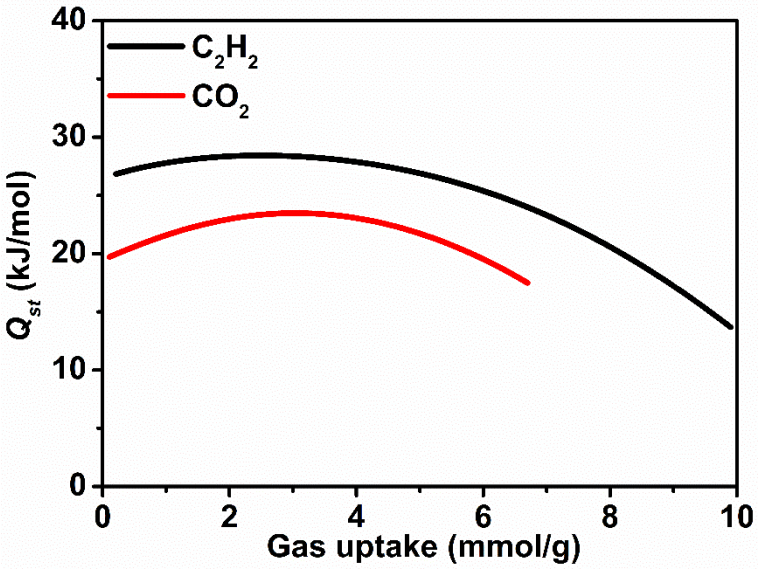

Figure S11. Calculated C_2H_2 and CO_2 adsorption enthalpy (Q_{st}) of JNU-4a.

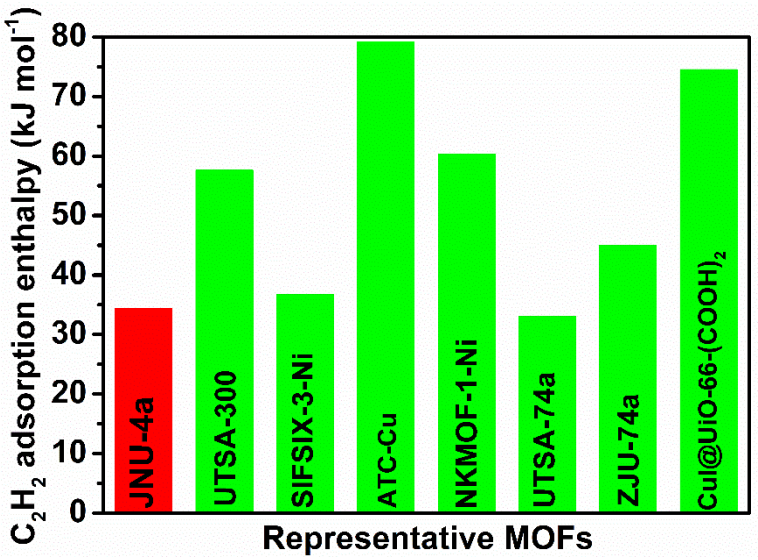

Figure S12. The maximum C_2H_2 adsorption enthalpy of JNU-4a and some selected high-performance MOFs.

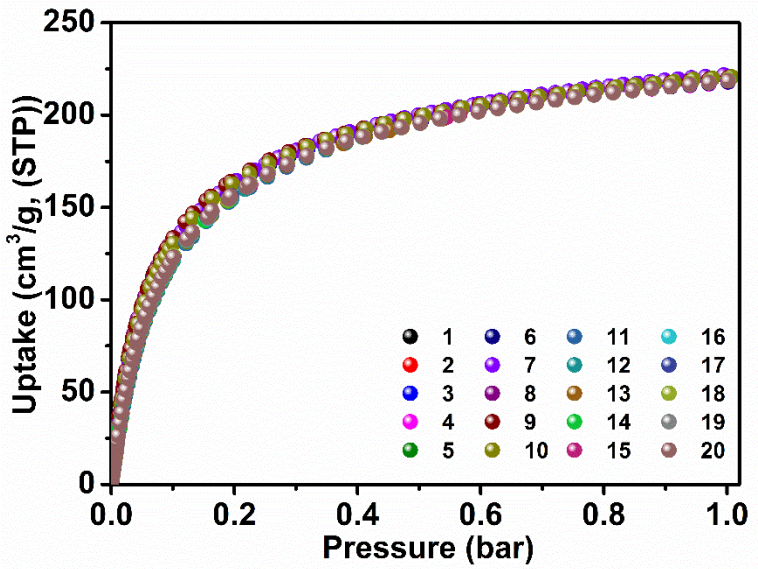

Figure S13. Continuous C_2H_2 adsorption measurements on JNU-4a at 298 K.

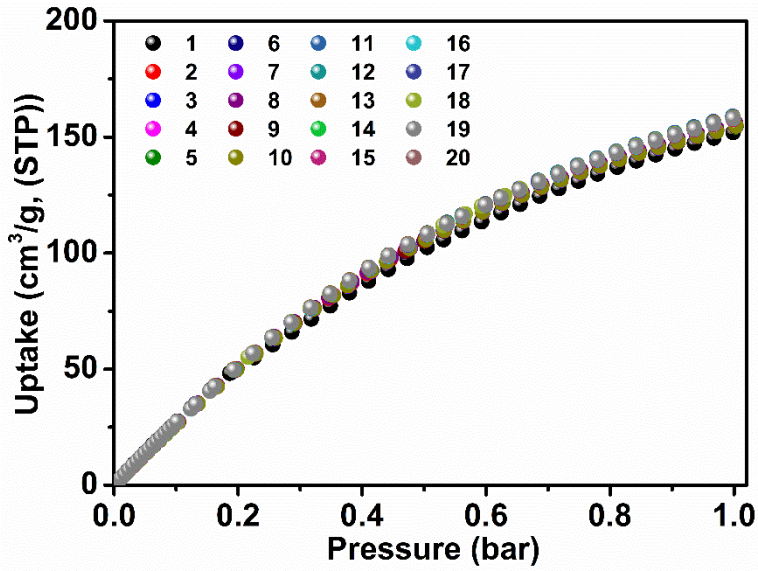

Figure S14. Continuous CO_2 adsorption measurements on JNU-4a at 298 K.

Theoretical Calculations

To better study the C_2H_2 adsorption and separation mechanism, Grand Canonical Monte Carlo (GCMC) simulations were performed to simulate the single-component adsorption of C_2H_2 and CO_2 on JNU-4a at 298 K and pressure up to 1 bar. The framework of JNU-4a was regarded as rigid during the simulation. The Lennard-Jones (LJ) parameters of JNU-4a were taken from the universal force field (UFF),[6] whereas C_2H_2 and CO_2 molecules were obtained from literatures.[7,8] The LJ parameters of different atom types were computed using the Lorentz-Berthelot mixing rules. The cut-off radius was chosen as 13 Å for the LJ potential, and the long-range electrostatic interactions were handled using Ewald summation technique. The equilibration steps and production steps were both set as 1.0×10^7. The DDEC charges[9] calculated by the Vienna ab initio simulation package (VASP),[10],[11] were employed to the framework atoms. Perdew-Burke-Ernzerhof (PBE) functional with generalized gradient approximation (GGA) was used to evaluate the electron exchange correlation. The radial distribution functions g(r) for host-guest atomic pairs at 298 K and 1 bar were further studied by Monte Carlo simulation in canonical (NVT) ensemble. All the simulations were performed by RASPA2 software.[12],[13]

To further quantify the binding energies between framework and gas molecules, dispersion-corrected density functional theory (DFT-D) calculations were performed based on the cluster models extracted from the structures of JNU-4a. The truncated bonds of the cluster models were saturated with hydrogen atoms or methyl groups. All geometry optimizations were performed at the B3LYP-D3/6-31+G(d, p) level for the non-metal atoms.[14-16] For Cu atom, the LanL2DZ basis set[17] was used to consider the relativistic effects. Frequency analyses were performed at the same computational level to confirm local minima for each optimized structure. Based on the optimized geometries, these binding energies (ΔE) were corrected from the basis set superposition error (BSSE) by the counterpoise procedure.[18] All these DFT-D calculations were accomplished using Gaussian 16 software.[19]

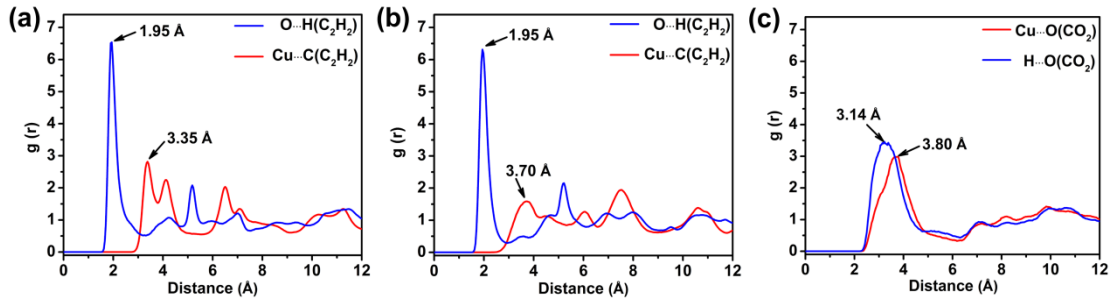

Figure S15. (a) Radial distribution function (RDF) of C_2H_2 at site I. (b) Radial distribution function (RDF) of C_2H_2 at site II. (c) Radial distribution function (RDF) of CO_2 at site I.

Column breakthrough experiments

The mixed-gas breakthrough separation experiments were conducted by using an in-house assembled system at 298 K and 1 bar (**Figure S16**). In a typical breakthrough experiment for C_2H_2/CO_2 (50:50) gas mixture, JNU-4a powder (0.82 g) was packed into a custom-made stainless-steel column (3.15 mm internal diameter × 450 mm long) with silica wool filling the void space. The sorbent was activated in-situ in the column with a high vacuum at 298 K for 24 h. After the activation process, a helium flow (50 mL min^{-1}) was introduced to purge the adsorbent. The flow of helium was then turned off and a gas mixture of C_2H_2/CO_2 (50:50) was allowed to flow into the column. Outlet effluent from the column was continuously monitored using gas chromatography (GC-7890B, Agilent) with a thermal conductivity detector (TCD). After the breakthrough experiment, the sample was regenerated in-situ in the column with a helium flow (100 mL min^{-1}) at 298 K for 6 h.

The completion of breakthrough was indicated by the downstream gas compositions reaching those in the feed gas. On the basis of the mass balance, the gas adsorption capacities can be determined as follows:[20]

$$q_i = \frac{C_i V}{22.4 \times m} \times \int_0^t (1 - \frac{F}{F_0})\, dt$$

Where q_i is the equilibrium adsorption capacity of gas i (mmol g^{-1}), C_i is the feed gas concentration, V is the volumetric feed flow rate (mL min^{-1}), t is the adsorption time (min), F_0 and F are the inlet and outlet gas molar flow rates, respectively, and m is the mass of the adsorbent (g). The separation factor (α) of the breakthrough experiment is determined as:

$$\alpha = \frac{q_A y_B}{q_B y_A}$$

in which y_i is the molar fraction of gas i (i = A, B) in the gas mixture.

The C_2H_2 purity (c) is defined by the peak area of C_2H_2, we calculated C_2H_2 purity according to the following equation:

$$c = \frac{C_i(C_2H_2)}{C_i(C_2H_2) + C_i(CO_2)}$$

where $C_i(CO_2)$ and $C_i(C_2H_2)$ represent the peak areas of component CO_2 and C_2H_2 in a single injection.

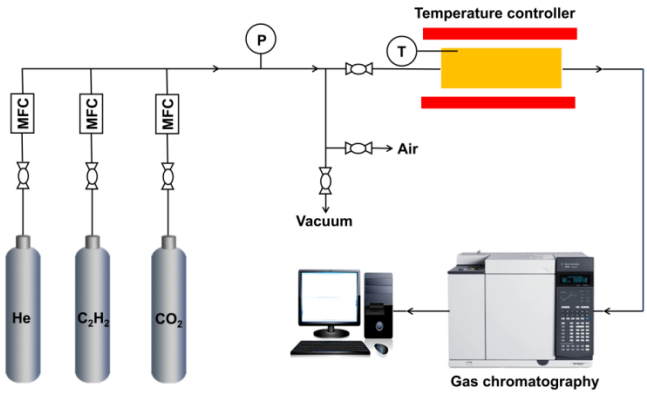

Figure S16. Schematic illustration of the setup for breakthrough experiments.

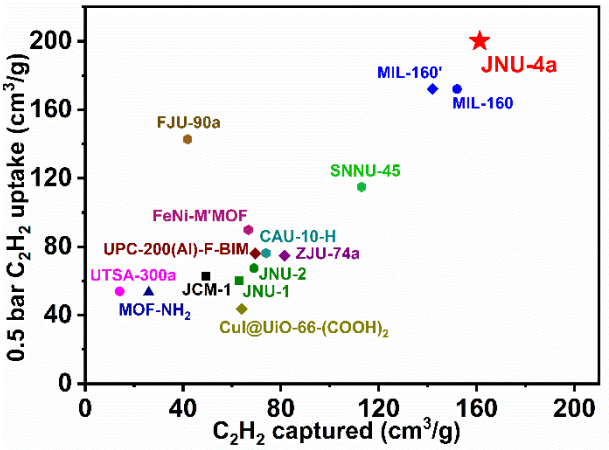

Figure S17. Comparison of the estimated amount of C_2H_2 captured on breakthrough column for an equimolar mixture of C_2H_2/CO_2 (JNU-4a and other top-performing materials).

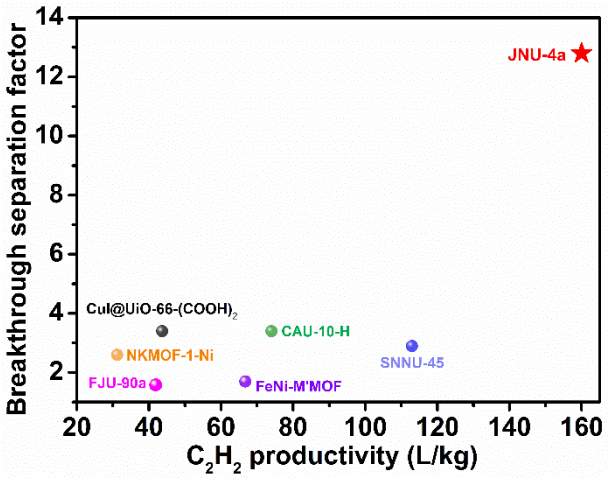

Figure S18. Comparison of the estimated amount of C_2H_2 captured and separation factor on breakthrough column for an equimolar mixture of C_2H_2/CO_2 in JNU-4a and other top-performing materials.

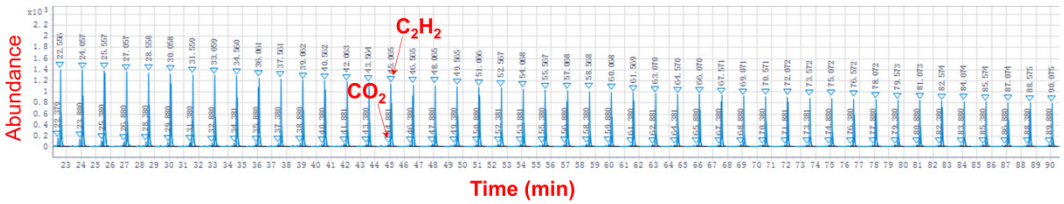

Figure S19. Desorption curve and its corresponding GC chromatogram for JNU-4a with C_2H_2/CO_2 (50/50, 4 mL min^{-1}) as feed gas.

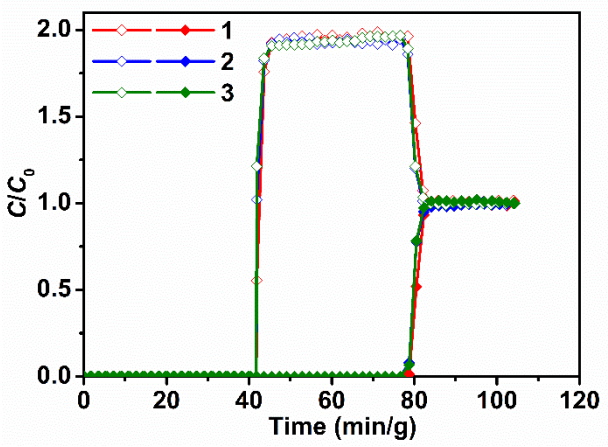

Figure S20. Breakthrough curves (from 1 to 3) for a C_2H_2/CO_2 (50:50) mixture flowing through a fixed column packed with JNU-4a at 298 K (flowrate: 4 mL min^{-1}).

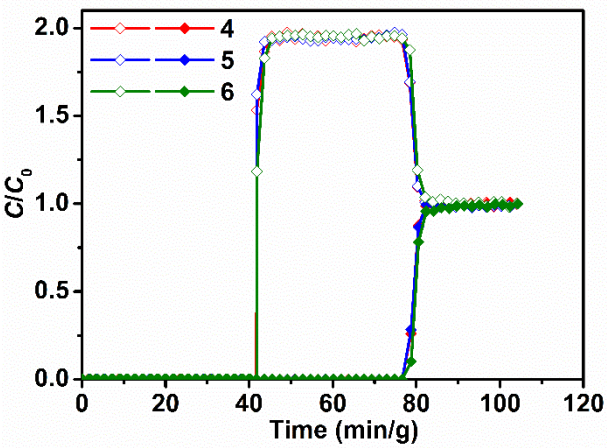

Figure S21. Breakthrough curves (from 4 to 6) for a C_2H_2/CO_2 (50:50) mixture flowing through a fixed column packed with JNU-4a at 298 K (flowrate: 4 mL min^{-1}).

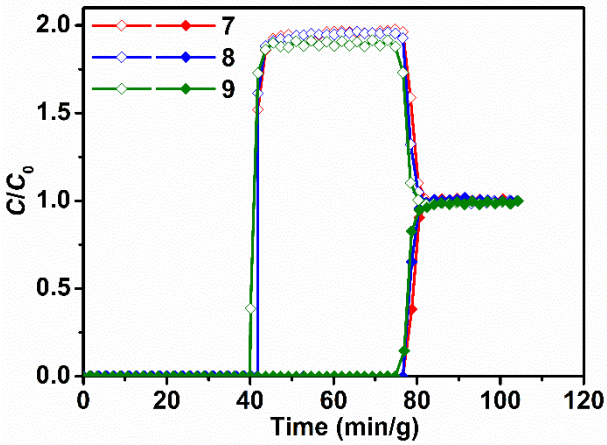

Figure S22. Breakthrough curves (from 7 to 9) for a C_2H_2/CO_2 (50:50) mixture flowing through a fixed column packed with JNU-4a at 298 K (flowrate: 4 mL min^{-1}).

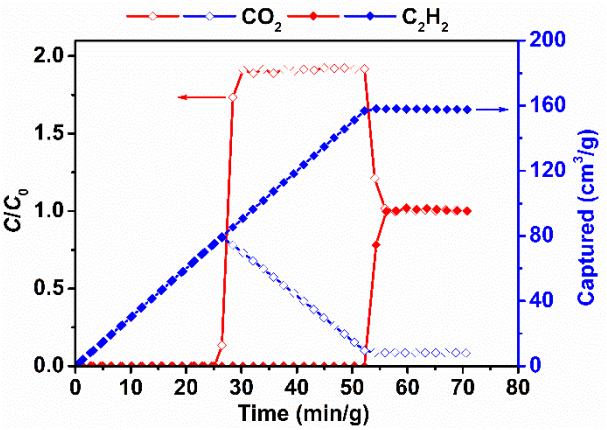

Figure S23. Breakthrough curves (left *y*-axis) of C_2H_2 and CO_2 on JNU-4a for an equimolar mixture of C_2H_2/CO_2 (6.0 mL min^{-1}) at 298 K. Empty squares depict the estimated amount of C_2H_2 and CO_2 captured on breakthrough column (right *y*-axis).

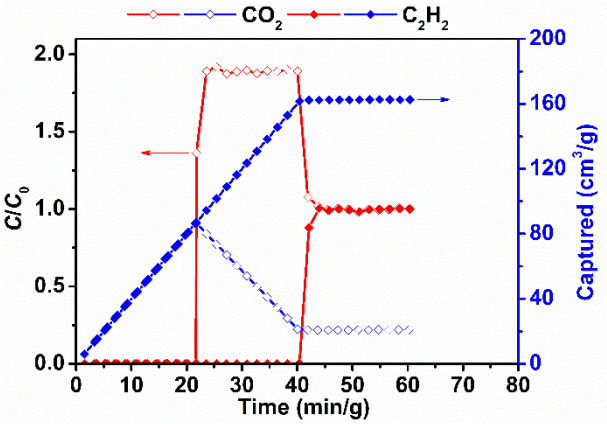

Figure S24. Breakthrough curves (left *y*-axis) of C_2H_2 and CO_2 on JNU-4a for an equimolar mixture of C_2H_2/CO_2 (8.0 mL min^{-1}) at 298 K. Empty squares depict the estimated amount of C_2H_2 and CO_2 captured on breakthrough column (right *y*-axis).

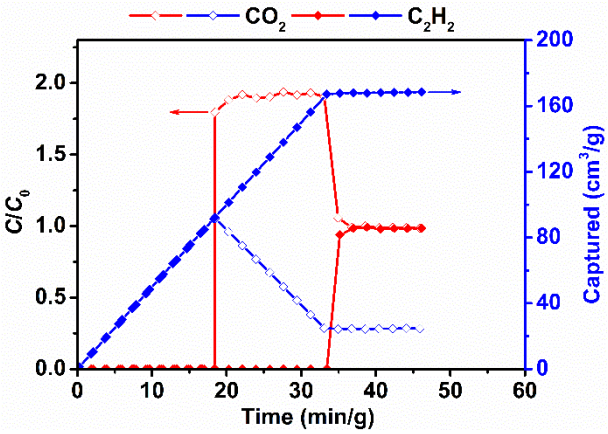

Figure S25. Breakthrough curves (left *y*-axis) of C_2H_2 and CO_2 on JNU-4a for an equimolar mixture of C_2H_2/CO_2 (10.0 mL min^{-1}) at 298 K. Empty squares depict the estimated amount of C_2H_2 and CO_2 captured on breakthrough column (right *y*-axis).

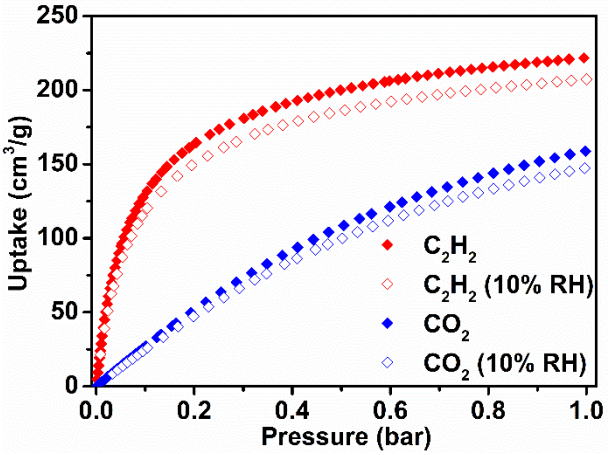

Figure S26. Adsorption isotherms of C_2H_2 (red) and CO_2 (blue) at 298 K and up to 1 bar under dry (0% RH) and humid conditions (10% RH).

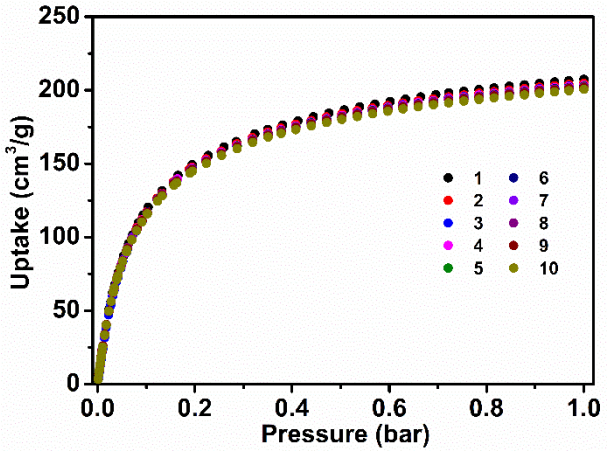

Figure S27. (a) Continuous adsorption measurements of C_2H_2 with 10% RH on JNU-4a at 298 K.

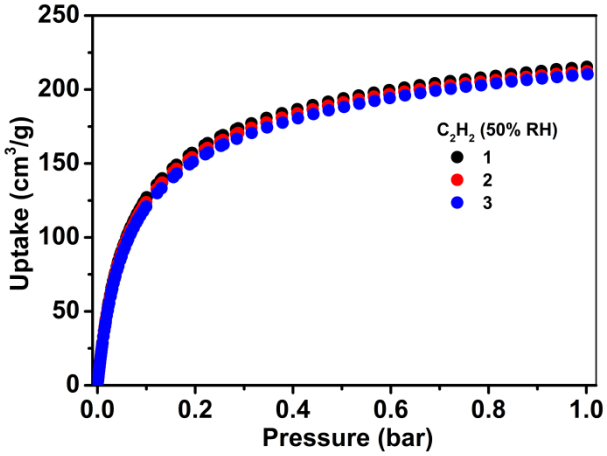

Fig. S28. Three consecutive adsorption measurements of C_2H_2 on JNU-4a under 50% RH at 298 K.

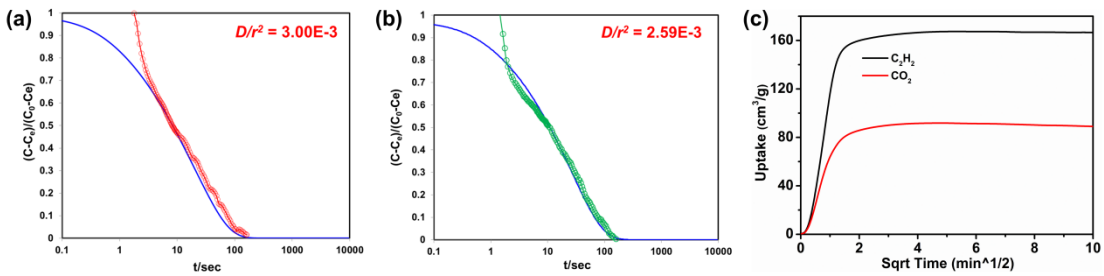

Fig. S29. Calculated diffusion rate constants of (a) C_2H_2 and (b) CO_2 in JNU-4a at 298 K, data were collected on a BEL MAX II sorption analyzer and fitted automatically with BEL-Master software according to the Crank theory. (c) Time-dependent C_2H_2 and CO_2 gravimetric adsorption on JNU-4a at 298 K, data were collected on a thermogravimetric analyzer (TGA) at a flow rate of 50 mL min^{-1} and 1.0 bar.

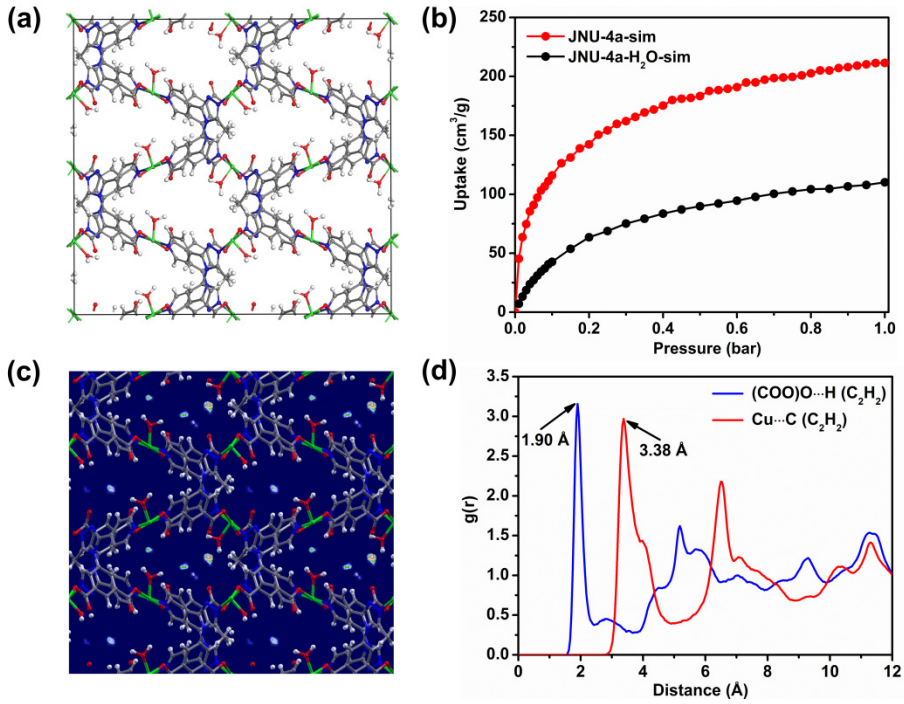

Fig. S30. (a) Crystal structure of JNU-4a-H_2O built by using the Forcite module embedded in Materials Studio 2018 (MS 2018). (b) Simulated C_2H_2 adsorption isotherms of JNU-4a and JNU-4a-H_2O at 298 K and up to 1 bar. (c) GCMC simulated adsorption density distributions of C_2H_2 in JNU-4a-H_2O at 298 K and 1 bar. (d) Radial distribution function (RDF) of C_2H_2 in JNU-4a-H_2O.

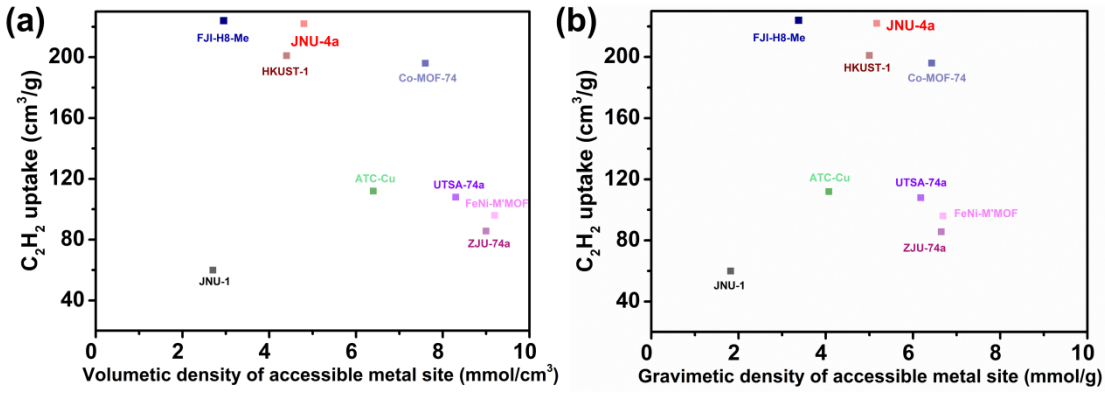

Fig. S31. Comparison of the (a) volumetric density and (b) gravimetric density of OMSs and C_2H_2 uptake in JNU-4a and some selected porous materials at room temperature.

Table S2. Summary of the adsorption capacity and Q_{st} of C_2H_2 and CO_2, as well as captured amount of C_2H_2 from 50:50 C_2H_2/CO_2 mixture in some selected MOFs (reorganized from refs. 21-37).

MOFs	C_2H_2 uptake (mmol/g)	CO_2 uptake (mmol/g)	Q_{st} of C_2H_2 (kJ/mol)	Q_{st} of CO_2 (kJ/mol)	Captured amount of C_2H_2	Ref
JCM-1	3.35	1.70	36.9	33.4	2.2	[21]
JNU-1	2.68	–	13-47.6	–	2.81	[22]
MAF-2	3.125	0.85	29.8-33.7	25.8-26.9	–	[23]
UTSA-74a	4.82	3.0	31	25	–	[24]
UTSA-300a	3.1	0.183	57.6	–	0.63	[25]
MFM-188	10.35	5.36	32.5	21	–	[26]
SIFSIX-3-Ni	3.3	2.7	36.7	50.9	–	[27]
MOF-NH_2	2.67	1.4	17.6	24.2	1.16	[28]
MOF-OH	3.04	1.2	16.8	20.6	1.25	[28]
ZJU-74a	3.83	3.02	65	32	3.64	[29]
UPC-200(Al)-F-BIM	6.45	2.48	20.5	–	3.1	[30]
CuI@UiO-66-COOH	2.31	0.93	74.5	28.9	2.89	[31]
FJI-H8-Me	10.2	4.73	33.70	21.77	–	[32]
SNNU-27-Fe	8.14	2.92	24.1	19.8	–	[33]
CAU-10-H	4.01	2.68	27	–	3.3	[34]
ATC-Cu	5.01	4.02	79.1	–	–	[35]
FJU-90a	8.04	4.6	25.1	20.7	1.87	[36]
SNNU-45	6.0	4.35	40	27	5.04	[33]
FeNi-M'MOF	4.29	2.72	27 ~ 32.8	24.5	2.98	[37]
MIL-160	8.53	4.01	31.8	26.9	6.8	[38]
JNU-4a	9.82	7.1	13.7 ~ 28.4	17.5 ~ 23.4	7.1	This work

Table S3. Crystal data of JNU-4.

	JNU-4
Temperature	100 K
Formula	C16H10CuN4O4[+ Solvent]
CCDC number	2160960
Space group	*P* 2_1/c
Crystal system	monoclinic
a (Å)	14.23(1)
b (Å)	13.23(1)
c (Å)	14.62(2)
α (deg)	90
β (deg)	93.15(1)
γ (deg)	90
V (Å)^3	2751.90(5)
Z	4
ρ calcg/cm^3	1.336
μ/mm^{-1}	1.557
Final R	R1=0.1134
[I>2sigma (I)]	wR1=0.2955
GooF	1.049
Completeness	100%

Table S4. Summary of C_2H_2 adsorption capacity from a 50:50 C_2H_2/CO_2 mixture in some selected MOFs and their respective experimental parameters.

Material	Column size (D × L, mm)	Flow rate (mL/min)	Packing density	Temperature (^oC)	Adsorption capacity (cm^3/g)
JNU-4a	3.15 × 450	4	–	25	160
MIL-160	4 × 150	2	–	25	152
FeNi-M'MOF	4 × 150	2	–	25	66.7
CuI@UiO-66-$(COOH)_2$	4.6 × 100	2	–	25	64.7
ZJU-74	4 × 120	2	–	25	81.5
SNNU-45	40 × 120	4	–	25	112.8
UPC-200(Al)-F-BIM	–	4	–	25	69
CAU-10-H	4 × 90	2	–	25	74

Table S5. Comparison of the volumetric density of OMSs and C_2H_2 uptake in JNU-4a and some other MOFs.

MOF	Formula	Formula weight (g mol^{-1})	Density (g cm^{-3})	Volumetric density of OMSs (mmol cm^{-3})	Gravimetric density of OMSs (mmol g^{-3})	C_2H_2 uptake (cm^3 g^{-1})
JNU-1	$Zn_3C_{14}H_8N_6O_6$	552.4	1.484	2.7	1.82	60
FJI-H8	$CuC_{11.5}H_{5.5}O_{5.5}$	295	0.873	2.95	3.38	224
HKUST-1	$Cu_3C_{18}H_6O_{12}$	604.87	0.879	4.4	5.0	201
JNU-4a*	$CuC_{16}H_{10}N_4O_4$	385.5	0.928	4.8	5.17	222 (This work)
ATC-Cu	CuC_9H_7O	242.69	1.571	6.4	4.07	112
Co-MOF-74	$Co_2C_8H_2O_6$	311.96	1.181	7.6	6.43	196
UTSA-74a*	$Zn_2C_8H_2O_6$	324.88	1.342	8.3	6.18	108
ZJU-74*	$NiC_8H_4CoN_6$	301.81	1.353	9.0	6.65	85.7
FeNiM'MOF*	$FeNiC_8H_4N_6$	298.70	1.375	9.2	6.69	96

*Note that every open metal center in these MOFs have two accessible sites.

References

[1] Dinca, M.; Dailly, A.; Liu, Y.; Brown, C. M.; Neumann, D. A.; Long, J. R. *J. Am. Chem. Soc.* **2006**, 128, 16876−16883.

[2] Myers, A. L.; Prausnitz, J. M. *AIChE J.* **1965**, 11, 121−127.

[3] Xie, Y.; Cui, H.; Wu, H.; Lin, R. B.; Zhou, W.; Chen, B., *Angew. Chem. Int. Ed.* **2021**, 60, 9604-9609.

[4] Graham, C.; Pierrus, J.; Raab, R. E. *Mol. Phys.* **1989**, 67, 939−955.

[5] Zhang, J.; Lu, T. *Phys. Chem. Chem. Phys.* **2021**, *23*, 20323–2032.

[6] Rappé, A. K.; Casewit, C. J.; Colwell, K. S.; Goddard, W. A.; Skiff, W. M. *J. Am. Chem. Soc.* **1992**, 114, 10024−10035.

[7] Jorgensen, W. L.; Madura, J. D.; Swenson, C. J. *J. Am. Chem. Soc.* **1984**, 106, 6638−6646.

[8] Garcia-Sanchez, A.; Ania, C. O.; Parra, J. B.; Dubbeldam, D.; Vlugt, T. J. H.; Krishna, R.; Calero, S. *J. Phys. Chem. C* **2009**, 113, 8814−8820.

[9] Manz, T. A.; Sholl, D. S. *J. Chem. Theory Comput.* **2010**, 6, 2455−2468

[10] Kresse, G.; Furthmuller, J. *Phys. Rev. B: Condens. Matter Mater. Phys.* **1996**, 54, 11169−11186.

[11] Kresse, G.; Joubert, D. *Phys. Rev. B: Condens. Matter Mater. Phys.* **1999**, 59, 1758−1775.

[12] D. Dubbeldam, A. Torres-Knoop, K. S. Walton, *Mol. Simul.* **2013**, *39*, 1253−1292.

[13] Dubbeldam, D.; Calero, S.; Ellis, D. E.; Snurr, R. Q. RASPA: *Mol. Simul.* **2016**, 42, 81−101.

[14] Becke, A. D. *J. Chem. Phys.* **1992**, 96, 2155−2160.

[15] Grimme, S.; Antony, J.; Ehrlich, S.; Krieg, H. *J. Chem. Phys.* **2010**, 132, 154104.

[16] Hariharan, P. C.; Pople, J. A. *Theoretica Chimica Acta* **1973**, 28, 213−222.

[17] Roy, L. E.; Hay, P. J.; Martin, R. L. *J. Chem. Theory Comput.* **2008**, 4, 1029−1031.

[18] Boys, S. F.; Bernardi, F. *Mol. Phys.* **1970**, 19, 553−566.

[19] Frisch, M. J.; Trucks, G. W.; Schlegel, H. B.; Scuseria, G. E.; Robb, M. A.; Cheeseman, J. R.; Scalmani, G.; Barone, V.; Petersson, G. A.; Nakatsuji, H.; et al., Gaussian 16, revision B.01; Gaussian, Inc.: Wallingford, CT, **2016**. 66.

[20] Liu, J.; Tian, J.; Thallapally, P. K.; McGrail, B. P. *J. Phys. Chem. C* **2012**, 116, 9575.

[21] Wang, L.; Sun, W.; Zhang, Y.; Xu, N.; Krishna, R.; Hu, J.; Jiang, Y.; He, Y.; Xing, H. *Angew. Chem. Int. Ed.* **2021**, 60, 22865−22870.

[22] Zeng, H.; Xie, M.; Huang, Y. L.; Zhao, Y.; Xie, X. J.; Bai, J. P.; Wan, M. Y.; Krishna, R.; Lu, W.; Li, D. *Angew. Chem. Int. Ed.* 2019, 58, 8515−8519.

[23] Zhang, J.-P.; Chen, X.-M. *J. Am. Chem. Soc.* **2009**, 131, 5516−5521.

[24] F. Luo, C. Yan, L. Dang, R. Krishna, W. Zhou, H. Wu, X. Dong, Y. Han, T.-L. Hu, M. OKeeffe, L. Wang, M. Luo, R.-B. Lin, B. Chen, *J. Am. Chem. Soc.* **2016**, 138, 5678–5684.

[25] Lin, R. B.; Li, L.; Wu, H.; Arman, H.; Li, B.; Lin, R. G.; Zhou, W.; Chen, B. *J. Am. Chem. Soc.* **2017**, 139, 8022−8028.

[26] Moreau, F.; da Silva, I.; Al Smail, N. H.; Easun, T. L.; Savage, M.; Godfrey, H. G.; Parker, S. F.; Manuel, P.; Yang, S.; Schroder, M. *Nat. Commun.* **2017**, 8, 14085.
[27] K.-J. Chen, H. S. Scott, D. G. Madden, T. Pham, A. Kumar, A.Bajpai, M. Lusi, K. A. Forrest, B. Space, J. J. Perry, M. J. Zaworotko, *Chem* **2016**. 1, 753–765.
[28] Gong, W.; Cui, H.; Xie, Y.; Li, Y.; Tang, X.; Liu, Y.; Cui, Y.; Chen, B. *J. Am. Chem. Soc.* **2021**, 143, 14869−14876.
[29] J. Pei, K. Shao, J. X. Wang, H. M. Wen, Y. Yang, Y. Cui, R. Krishna, B. Li, G. Qian, *Adv. Mater.* **2020**, 32, 1908275.
[30] Fan, W.; Yuan, S.; Wang, W.; Feng, L.; Liu, X.; Zhang, X.; Wang, X.; Kang, Z.; Dai, F.; Yuan, D.; Sun, D.; Zhou, H. C. *J. Am. Chem. Soc.* **2020**, 142, 8728−8737.
[31] Zhang, L.; Jiang, K.; Yang, L.; Li, L.; Hu, E.; Yang, L.; Shao, K.; Xing, H.; Cui, Y.; Yang, Y.; Li, B.; Chen, B.; Qian, G. *Angew. Chem., Int. Ed.* **2021**, 60, 15995−16002.
[32] Di, Z.; Liu, C.; Pang, J.; Chen, C.; Hu, F.; Yuan, D.; Wu, M.; Hong, M. *Angew. Chem., Int. Ed.* **2021**, 60, 10828−10832.
[33] Xue, Y.-Y.; Bai, X.-Y.; Zhang, J.; Wang, Y.; Li, S.-N.; Jiang, Y.-C.; Hu, M.-C.; Zhai, Q.-G. *Angew. Chem., Int. Ed.* **2021**, 60, 10122−10128.
[34] Pei, J.; Wen, H. M.; Gu, X. W.; Qian, Q. L.; Yang, Y.; Cui, Y.; Li, B.; Chen, B.; Qian, G. *Angew. Chem, Int. Ed.* 2021, 133, 2−9.
[35] Niu, Z.; Cui, X.; Pham, T.; Verma, G.; Lan, P. C.; Shan, C.; Xing, H.; Forrest, K. A.; Suepaul, S.; Space, B.; Nafady, A.; Al-Enizi, A. M.; Ma, S. *Angew. Chem., Int. Ed.* **2021**, 60, 5283−5288.
[36] Ye, Y.; Ma, Z.; Lin, R.-B.; Krishna, R.; Zhou, W.; Lin, Q.; Zhang, Z.; Xiang, S.; Chen, B. *J. Am. Chem. Soc.* **2019**, 141, 4130−4136.
[37] Gao, J.; Qian, X.; Lin, R.-B.; Krishna, R.; Wu, H.; Zhou, W.; Chen, B. *Angew. Chem., Int. Ed.* **2020**, 59, 4396−4400.
[38] Ye, Y.; Xian, S.; Cui, H.; Tan, K.; Gong, L.; Liang, B.; Pham, T.; Pandey, H.; Krishna, R.; Lan, P. C.; Forrest, K. A.; Space, B.; Thonhauser, T.; Li, J.; Ma, S. *J. Am. Chem. Soc.* **2022**, 144, 1681−1689.